Numerical simulations of conversion to Alfvén waves in sunspots

E. Khomenko[1,2] and P. S. Cally[3]

khomenko@iac.es

paul.cally@monash.edu

ABSTRACT

We study the conversion of fast magneto-acoustic waves to Alfvén waves by means of 2.5D numerical simulations in a sunspot-like magnetic configuration. A fast, essentially acoustic, wave of a given frequency and wave number is generated below the surface and propagates upward though the Alfvén/acoustic equipartition layer where it splits into upgoing slow (acoustic) and fast (magnetic) waves. The fast wave quickly reflects off the steep Alfvén speed gradient, but around and above this reflection height it partially converts to Alfvén waves, depending on the local relative inclinations of the background magnetic field and the wavevector. To measure the efficiency of this conversion to Alfvén waves we calculate acoustic and magnetic energy fluxes. The particular amplitude and phase relations between the magnetic field and velocity oscillations help us to demonstrate that the waves produced are indeed Alfvén waves. We find that the conversion to Alfvén waves is particularly important for strongly inclined fields like those existing in sunspot penumbrae. Equally important is the magnetic field orientation with respect to the vertical plane of wave propagation, which we refer to as "field azimuth". For field azimuth less than 90° the generated Alfvén waves continue upwards, but above 90° downgoing Alfvén waves are preferentially produced. This yields negative Alfvén energy flux for azimuths between 90° and 180°. Alfvén energy fluxes may be comparable to or exceed acoustic fluxes, depending upon geometry, though computational exigencies limit their magnitude in our simulations.

Subject headings: Sun: oscillations – Sun: sunspots – Sun: numerical simulations

[1]Instituto de Astrofísica de Canarias, 38205, C/ Vía Láctea, s/n, La Laguna, Tenerife, Spain

[2]Departamento de Astrofísica, Universidad de La Laguna, 38205, La Laguna, Tenerife, Spain

[3]School of Mathematical Sciences and Monash Centre for Astrophysics, Monash University , Clayton, Victoria, 3800 , Australia

1. Introduction

Observations using the Solar Optical Telescope (SOT) aboard *Hinode* (De Pontieu et al. 2007) and the Coronal Multi-Channel Polarimeter (CoMP) (Tomczyk et al. 2007) unambiguously reveal ubiquitous Alfvénic oscillations in the solar corona, with implications both for the Sun's atmosphere and the solar wind. Tomczyk et al. find that coronal Alfvénic power is broadly spread in frequency, but with a distinct peak around 3-4 mHz, characteristic of the Sun's internal p-mode wavefield. Whether these transverse oscillations are strictly Alfvén waves or instead kink waves (Van Doorsselaere et al. 2008) depends on the magnetic and density structuring of the atmosphere, and may vary with height as cross-field structuring becomes more or less important. We might expect though that sunspot atmospheres, with their presumed large-scale magnetic structures, present the most ideal site for more-or-less pure Alfvén waves to propagate.

The generation of Alfvén waves at the photosphere and their propagation through the various layers of the solar atmosphere has been extensively modelled (e.g. Cranmer & van Ballegooijen 2005). However, Cally & Hansen (2011) recently suggested that Alfvén waves must also be produced by mode conversion from fast magneto-acoustic waves beyond their reflection height in the low chromosphere. This coupling only occurs if wave propagation is not coplanar with gravity and magnetic field, and so the problem is necessarily three dimensional (3D).

Conversion from fast-mode high-β magneto-acoustic waves (manifesting as p modes in the subphotosphere) to slow-mode waves in solar active regions is relatively well studied both analytically and numerically (e.g., Zhugzhda & Dzhalilov 1982; Cally & Bogdan 1997; Cally 2001; Schunker & Cally 2006; Cally 2006, 2007; Hansen & Cally 2009; Khomenko et al. 2009; Felipe et al. 2010); see Khomenko (2009) for a review. In a two-dimensional situation, the transformation from fast to slow magnetoacoustic modes is demonstrated to be particularly strong for a narrow range of magnetic field inclinations around 20–30 degrees to the vertical. For this reason, and because of the reduction in acoustic cutoff frequency afforded by strong inclined magnetic fields, magnetic field concentrations on the solar surface may truly be called *magnetoacoustic portals* (Jefferies et al. 2006), coupling the Sun's interior oscillations to those of its atmosphere.

The remainder of the wave-energy flux though, which is near-total away from these preferred inclinations, enters the low-β atmosphere as fast, predominantly magnetic waves. Due to the steep Alfvén speed gradient with height, these fast waves soon reflect back downward at the height $z_{\rm ref}$ at which $\omega \approx v_A k_h$, where ω is the frequency, v_A the Alfvén speed, and k_h the horizontal wavenumber.

Fast-to-Alfvén conversion occurs around and above this fast wave reflection height $z_{\rm ref}$ in 3D (see Fig. 1), localized more closely to $z_{\rm ref}$ as frequency increases (Cally & Hansen 2011). However, at the 3-5 mHz frequencies characteristic of p-modes, the process is typically spread over much of the chromosphere. Studies of fast-to-Alfvén conversion were initiated by Cally & Goossens (2008), who found that it is most efficient for preferred field inclinations from vertical between 30 and 40 degrees, and azimuth angles (the angle between the vertical magnetic and wave propagation planes) between 60 and 80 degrees, and that Alfvénic fluxes transmitted to the upper atmosphere can exceed acoustic fluxes in some cases. Newington & Cally (2010) studied the conversion properties of low-frequency ($\sim$ 1-2 mHz) gravity waves, showing that even larger magnetic field inclinations can support gravity wave to Alfvén conversion and resulting Alfvénic wave propagation to the upper atmosphere. In nonuniform magnetic field, the relevant angles for mode conversion, either fast-to-slow or fast-to-Alfvén, are those pertaining in the respective conversion regions. Fig. 1 summarizes the overall picture of conversion between the fast, slow and Alfvén waves.

Motivated by these recent studies, we attack the problem by means of 2.5D numerical simulations. The purpose of our analysis is to calculate the efficiency of the conversion from fast-mode high-β magneto-acoustic waves to Alfvén and slow waves in the upper atmosphere in a spreading sunspot-like magnetic field configuration. Our initial results on the conversion to Alfvén waves in simple field configurations were reported in Khomenko & Cally (2011). In the present work we extend our simulations to a more realistic case of a sunspot atmospheric models spanning the shallow subphotosphere (-5 Mm) to the high chromosphere ($+1.9$ Mm).

Above this layer, the transition region acts as a partial Alfvén wave reflector, affecting their distribution in the corona and solar wind and producing Alfvén turbulence via nonlinear coupling (Cranmer & van Ballegooijen 2005), but this is beyond the scope of our present modeling.

2. Simulation setup

We numerically solve the non-linear equations of ideal MHD using our code `Mancha` (Khomenko & Collados 2006; Khomenko et al. 2008; Felipe et al. 2010). The code solves non-linear equations for perturbations, the equilibrium state being explicitly removed from the equations. In this study, for simplicity, and coherence with previous studies (see Cally & Hansen 2011), we use a 2.5D approximation. This approximation means that we allow all vectors in three spatial directions, but the derivatives are taken only in two (one vertical and one horizontal) directions, so that our perturbations are only allowed to propagate in the $X-Z$ plane. In addition, the initial perturbation is kept small to approximate the linear regime.

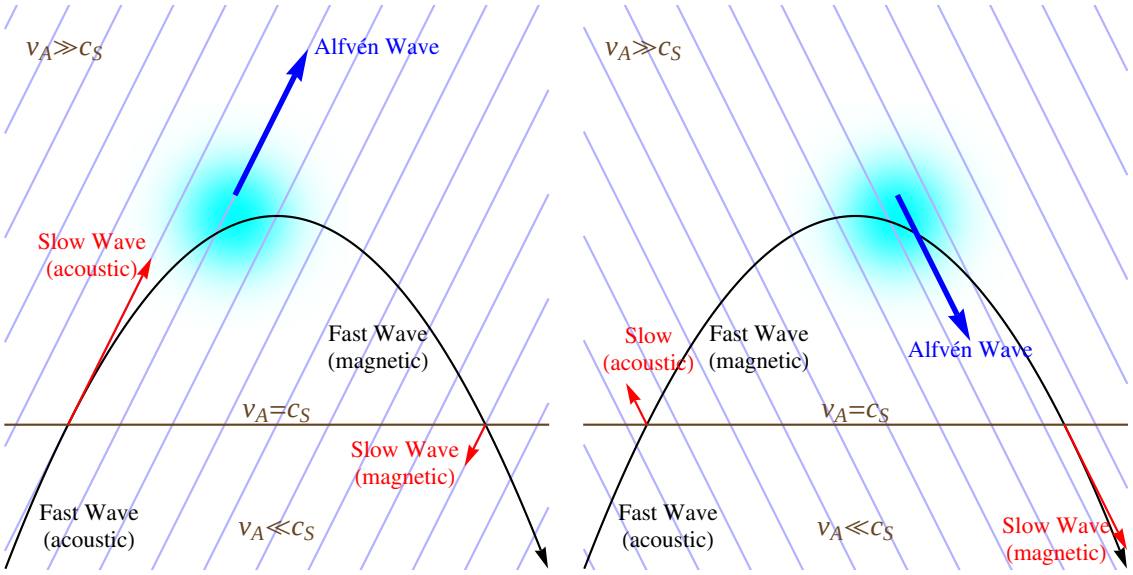

Fig. 1.— Schematic diagram illustrating the various mode conversions and reflections as a seismic ray (labeled "Fast Wave (acoustic)") enters the solar atmosphere in a region of strong inclined magnetic field. Field lines (pale blue) are oriented out of the plane and are shown here in projection. Their orientation is given by the inclination angle θ from vertical ($0 \leq \theta < 90°$) and azimuth angle ϕ measured clockwise from the wave propagation plane. By symmetry we need only consider $0 \leq \phi \leq 180°$, with $\phi < 90°$ in the left panel and $\phi > 90°$ in the right panel. First, at the Alfvén-acoustic equipartition level $v_A = c_S$ the ray splits into an essentially acoustic field-guided slow wave (depicted in red) and a fast magnetically dominated wave (black). The slow wave may or may not reflect depending on whether $\omega < \omega_c \cos\theta$. The fast wave goes on to reflect higher in the atmosphere due to the rapidly increasing Alfvén speed with height. On its way downward it again mode converts at the equipartition level. In the scenario depicted on the left ($\phi < 90°$), the upward slow wave is much stronger than the downward one because the fast ray is more closely aligned with the magnetic field (small attack angle) on the upstroke than on the downstroke. This situation is reversed if the magnetic field were inclined in the opposite direction (equivalent to $\phi > 90°$, right panel). In a nebulous region around and above the fast wave reflection point (which may extend far higher than the fuzzy blob used to represent it here), fast-to-Alfvén conversion occurs, in the case on the left predominantly to an upgoing Alfvén wave. For the $\phi > 90°$ (right), the downgoing Alfvén wave is favored. The fast-to-Alfven conversion may only occur where the wave vector and the magnetic field lines are not in the same vertical plane. This diagram extends the description in Cally (2007) by including fast-to-Alfvén conversion.

As a background magneto-static model atmosphere we use one sunspot-like model from Khomenko & Collados (2008). For simplicity, this model is azimuthally symmetric, with no twist of the magnetic field lines. Whilst twist is often seen in sunspot magnetic fields, it is not a necessary feature of the processes we wish to explore here. It will be added along with other physical features in later studies. The computational region is magnetized in all its volume (distributed currents), but the strongest magnetic field is concentrated around the axis of the structure. The dimensions of the simulated domain are 78 Mm in the horizontal X direction and 7.4 Mm in the vertical Z direction. The axis of the sunspot is placed at the middle of the domain at $X = 39$ Mm. The bottom boundary of the domain is located at -5 Mm below the photospheric level, $Z = 0$. This zero level is taken to be the height where the optical depth at 500 nm is equal to unity in the quiet Sun atmosphere 39 Mm away from the sunspot axis. The thermodynamic variables of the atmosphere at 39 Mm from the axis are taken from Model S of Christensen-Dalsgaard et al. (1996) in the deep sub-photosphere layers and continuing according to the VAL-C model (Vernazza et al. 1981) in the photospheric and chromospheric layers. The sunspot axis in the atmospheric layers is given by the semi-empirical model of Avrett (1981). The magnetic field at the axis is about 900 G at $Z = 0$ Mm. This is quite moderate for a sunspot, but is adopted for numerical reasons. The Alfvén speed at the top of our computational domain becomes quite excessive if the field strength is too high, thereby necessitating impractically small time steps. Taking larger field strength would mostly result in a different scaling of the problem, without new physical phenomena being introduced (see, e.g. Khomenko et al. 2009).

The spatial resolution of our simulations is 150 km in the horizontal direction and 50 km in the vertical direction (520 by 148 grid points). The upper 500 km (10 grid points) of the domain are occupied by the absorbing PML boundary layer (Khomenko et al. 2008; Felipe et al. 2010), so the effective physical boundary of the domain is located at 1.9 Mm above the photosphere. The PML, "Perfectly Matched Layer", is a numerical device that acts as an excellent absorber of waves, and thereby removes unphysical reflections from the edges of the computational domain. It is well-tested in the current code, and performs admirably. No significant reflections are detected. The concept of PML was firstly introduced by Berenger (1994) for electromagnetic waves, but was quickly extended to other wave types. It is now used in many codes modeling wave propagation, e.g. Parchevsky & Kosovichev (2007) and Hanasoge et al. (2010). The calculations throughout are adiabatic and we use the ideal equation of state to close the system.

As our modelling is 2.5D, we have made cuts through the sunspot model at several Y positions. Here we will describe three simulations situated in vertical planes at $Y = 7.5$, 11.25 and 15 Mm from the sunspot axis. A cut through the axis is uninteresting, as it is strictly 2D and can produce no Alfvén waves. Figure 2 depicts variations of some characteristic

parameters of the $Y = 7.5$ Mm cut through the sunspot model.

We drive waves by an imposed perturbation in a few grid points near the bottom boundary of the domain at $Z = -5$ Mm. The perturbation is calculated analytically as an acoustic-gravity wave of a given frequency and wavenumber, neglecting the magnetic field (dynamically unimportant at this depth), and neglecting the temperature gradient. We introduce self-consistent perturbations of the velocity vector, pressure, and density according to Mihalas & Mihalas (1984):

$$\begin{aligned}
\delta V_z &= V_0 \exp\left(\frac{z}{2H} + k_{zi} z\right) \sin(\omega t - k_{zr} z - k_x x) \\
\frac{\delta P}{P_0} &= V_0 |P| \exp\left(\frac{z}{2H} + k_{zi} z\right) \sin(\omega t - k_{zr} z - k_x x + \phi_P) \\
\frac{\delta \rho}{\rho_0} &= V_0 |R| \exp\left(\frac{z}{2H} + k_{zi} z\right) \sin(\omega t - k_{zr} z - k_x x + \phi_R) \\
\delta V_x &= V_0 |U| \exp\left(\frac{z}{2H} + k_{zi} z\right) \sin(\omega t - k_{zr} z - k_x x + \phi_U)\,,
\end{aligned} \tag{1}$$

where the amplitudes and relative phase shifts between the perturbations are given by

$$|P| = \frac{\gamma\omega}{\omega^2 - c_S^2 k_x^2} \sqrt{k_{zr}^2 + \left(k_{zi} + \frac{1}{2H}\frac{(\gamma-2)}{\gamma}\right)^2} \tag{2}$$

$$|R| = \frac{\omega}{\omega^2 - c_S^2 k_x^2} \sqrt{k_{zr}^2 + \left(k_{zi} + \frac{(\gamma-1)}{\gamma H}\frac{c_S^2 k_x^2}{\omega^2} - \frac{1}{2H}\right)^2} \tag{3}$$

$$|U| = \frac{k_x c_S^2}{\gamma\omega} |P| \tag{4}$$

$$\phi_P = \phi_U = \arctan\left(\frac{k_{zi}}{k_{zr}} + \frac{1}{2Hk_{zr}}\frac{(\gamma-2)}{\gamma}\right) \tag{5}$$

$$\phi_R = \arctan\left(\frac{k_{zi}}{k_{zr}} + \frac{(\gamma-1)}{\gamma H k_{zr}}\frac{c_S^2 k_x^2}{\omega^2} - \frac{1}{2Hk_{zr}}\right) \tag{6}$$

Given the wave frequency ω, and the horizontal wavenumber k_x, the vertical wavenumber k_z is found from the dispersion relation for acoustic-gravity waves in an isothermal atmosphere:

$$k_z = k_{zr} + i k_{zi} = \sqrt{(\omega^2 - \omega_c^2)/c_S^2 - k_x^2(\omega^2 - \omega_g^2)/\omega^2} \tag{7}$$

where $\omega_c = \gamma g / 2c_S$ is the acoustic cut-off frequency and $\omega_g = 2\omega_c\sqrt{\gamma - 1}/\gamma$.

In all simulations described in this work we set the perturbation frequency $\nu = \omega/2\pi = 5$ mHz and horizontal wave number $k_x = 1.37$ Mm^{-1}. According to our sunspot model (see Fig. 2), the driving frequency is just slightly below the maximum cut-off frequency

reached at the temperature minimum. Over most of the spot these values result in the fast wave reflection level $z_{\rm ref}$ being higher than the Alfvén/acoustic equipartition surface $z_{\rm eq}$, i.e., $\omega/k_x > c_S$ (automatically satisfied for a propagating acoustic wave $\omega^2 = c_S^2(k_x^2+k_z^2)$). This is important, since it allows upcoming acoustic (fast) waves in $v_A < c_S$ to convert to magnetic (fast) waves in $v_A > c_S$ before reflecting at $z_{\rm ref}$.

To separate the Alfvén mode from the fast and slow magneto-acoustic modes in the magnetically dominated atmosphere ($v_A \gg c_S$) we use velocity projections onto three characteristic directions:

$$\begin{aligned}\hat{e}_{\rm long} &= [\cos\phi\sin\theta,\ \sin\phi\sin\theta,\ \cos\theta];\\ \hat{e}_{\rm perp} &= [-\cos\phi\sin^2\theta\sin\phi,\ 1-\sin^2\theta\sin^2\phi,\\ &\qquad -\cos\theta\sin\theta\sin\phi];\\ \hat{e}_{\rm trans} &= [-\cos\theta,\ 0,\ \cos\phi\sin\theta].\end{aligned} \tag{8}$$

These projections were shown to be rather efficient in separating the perturbations corresponding to all three modes both for idealized magnetic field configurations (Khomenko & Cally 2011), and also for more complex ones (Felipe et al. 2010). The first projection ($\hat{e}_{\rm long}$) selects the slow magneto-acoustic wave, propagating parallel to the field; the second one ($\hat{e}_{\rm perp}$) selects the Alfvén wave, according to the asymptotic polarization direction derived by Cally & Goossens (2008); the remaining orthogonal direction ($\hat{e}_{\rm trans}$) selects the fast magneto-acoustic wave. In the rest of the paper we will address these projections as "acoustic", "Alfvén" and "fast".

To measure the efficiency of conversion to Alfvén waves near and above the $c_S = v_A$ equipartition layer, we calculate the time-averaged acoustic and magnetic energy fluxes as far as possible from the conversion layer in the magnetically dominated atmosphere ($v_A \gg c_S$):

$$\begin{aligned}\vec{F}_{\rm ac} &= \langle \delta P\, \delta\vec{V}\rangle\,,\\ \vec{F}_{\rm mag} &= \langle \delta\vec{B}\times(\delta\vec{V}\times\vec{B}_0)\rangle/\mu_0\,.\end{aligned} \tag{9}$$

The positive sign of the fluxes means energy propagating upwards.

We also calculate a measure of the time-averaged energy contained in all three wave modes according to

$$\begin{aligned}E_{\rm long} &= \rho_0 c_S \langle \delta V_{\rm long}^2\rangle\\ E_{\rm perp} &= \rho_0 v_A \langle \delta V_{\rm perp}^2\rangle\\ E_{\rm trans} &= \rho_0 v_A \langle \delta V_{\rm trans}^2\rangle\,,\end{aligned} \tag{10}$$

where in each case we use the corresponding velocity projections into characteristic directions (Eq. 8). For pure acoustic and Alfvén waves, where there is strict equipartition between

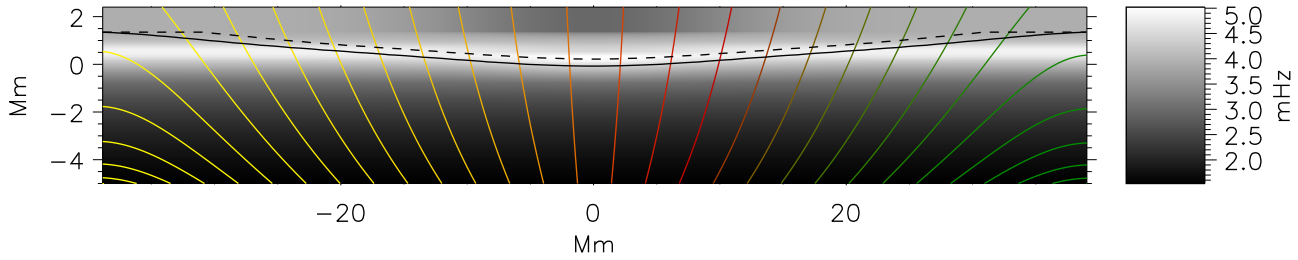

Fig. 2.— Properties of the magneto-static sunspot model in the $Y = 7.5$ Mm slice away from the axis. The background image is the acoustic cut-off frequency unadjusted for magnetic effects. The solid black line is the level where acoustic and Alfvén speeds are equal ($c_S = v_A$). The dashed line is the fast mode reflection level calculated as the level where the wave frequency ω and wave horizontal wave number k_x are related by $\omega = v_A k_x$. The magnetic field lines are shown as colored lines, different colors meaning different azimuth ϕ of the field from green ($\phi \approx 0°$) to red ($\phi \approx 90°$) and yellow ($\phi \approx 180°$); the ϕ is counted clockwise from the vertical wave propagation plane XZ.

Vertical and horizontal dimensions are not to scale.

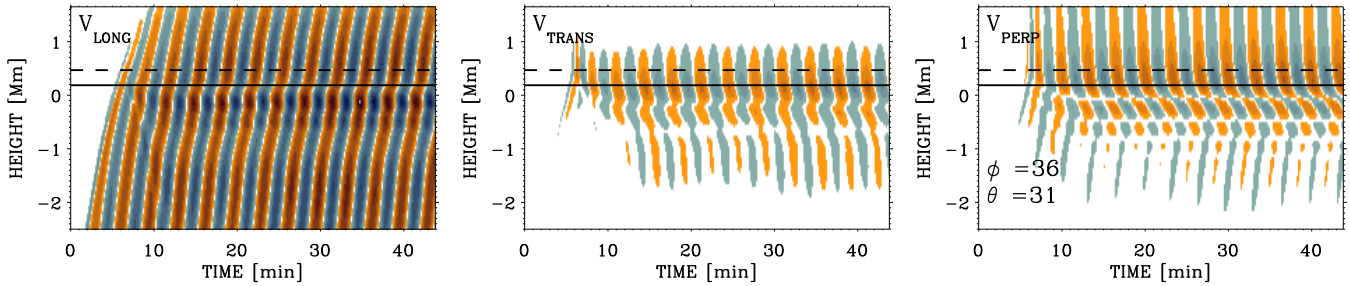

Fig. 3.— Variations with time (horizontal axis) and height (vertical axis) of the three orthogonal components of the velocity in the simulation at $Y = 7.5$ Mm from the sunspot axis. The color coding is the same in the three panels. The velocities are scaled with a factor of $\sqrt{\rho_0 c_S}$ (left panel) and $\sqrt{\rho_0 v_A}$ (middle and right panels). Horizontal solid line is the level where $c_S = v_A$; horizontal dashed line is the fast mode reflection level. Velocities are taken at one horizontal X location where the magnetic field inclination $\theta = 31°$ and azimuth $\phi = 36°$. While the fast mode (visible in $V_{\rm trans}$ above the $c_S = v_A$ level) is reflected, the Alfvén mode (visible in $V_{\rm perp}$ above the $c_S = v_A$ level) continues above. Note the difference in the propagation speeds of the acoustic and Alfvén wave above $c_S = v_A$.

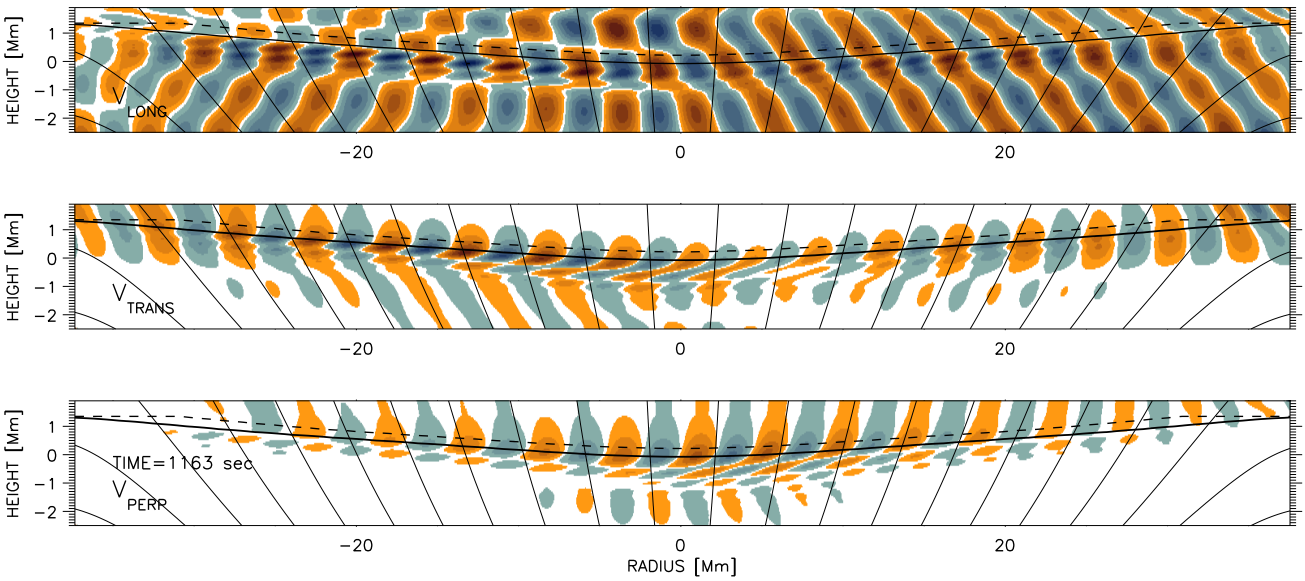

Fig. 4.— Snapshots of the three orthogonal components of the velocity taken at about 19 min after the start of the simulation at $Y = 7.5$ Mm from the sunspot axis. Upper panel: $V_{\rm long}$; middle panel: $V_{\rm trans}$; bottom panel: $V_{\rm perp}$. The blue-orange colors mean negative-positive velocity directions; the range of the color coding is the same in the three panels. The velocities are scaled with a factor of $\sqrt{\rho_0 c_S}$ (upper panel) and $\sqrt{\rho_0 v_A}$ (two lower panels). Horizontal solid line is the level where $c_S = v_A$; horizontal dashed line is the fast mode reflection level. Magnetic field lines are inclined black lines. The axes are not to scale. Note the presence of the Alfvén mode in $V_{\rm perp}$ above $c_S = v_A$, where the fast mode ($V_{\rm trans}$) is already reflected. Since the velocity polarizations 'long', 'trans', and 'perp' are based on $v_A \gg c_S$ asymptotics, care must be taken not to over-interpret these figures well below the equipartition level. The apparent "discontinuity" seen in $V_{\rm perp}$ near $Z = -1$ Mm (seen also in Fig. 3) is a node.

kinetic and compressional or kinetic and magnetic energies respectively, these would indeed be the true energies. Be that as it may, these forms are convenient for purposes of exposition and shall be used here.

3. Velocity projections

Figure 3 shows an example of the projected velocity components in our calculations as a function of height and time. The velocities are taken at $X = 10.5$ Mm, where the distinction between the three wave modes in the magnetically dominated atmosphere is clearly visible. In this representation the larger inclination of the ridges means lower propagation speeds and vice versa. Note, that projecting the velocities according to Eq. (8) allows us to separate the wave modes only in the magnetically dominated atmosphere, above the horizontal solid line in Fig. 3. The figure shows how the incident fast mode wave propagates to the equipartition layer $c_S = v_A$ gradually changing its speed. After reaching the equipartition layer at about 5 min into the simulation, it splits into several components. The essentially magnetic low-β fast mode is produced above $Z = 0.2$ Mm (middle panel). This mode is reflected back down a few minutes after it has been produced. The reflection height, calculated as the height where the wave frequency ω and wave horizontal wave number k_x are related by $\omega = v_A k_x$ (ignoring the sound speed contribution to the fast wave speed), is well reproduced in the simulations, as the velocity variations associated with the fast mode decay rapidly above its reflection layer.

Unlike the purely 2D case, there is an Alfvén mode produced above the $c_S = v_A$ level (right panel). This mode has a clearly distinct propagation speed compared to the acoustic mode (left panel). The ridges of the Alfvén mode are nearly vertical since the Alfvén speed at these heights is large (above 100 $\mathrm{km\,s^{-1}}$).

The low-β essentially acoustic slow mode escapes to the upper atmosphere tunnelling through the cut-off layer due to the field inclination of $\theta = 30^\circ$ that effectively reduces the cut-off frequency by the factor $\cos\theta$.

The velocity amplitudes in Fig. 3 are scaled with a factor of $\sqrt{\rho_0 v_{\rm ph}}$, where $v_{\rm ph} = c_S$ for the $V_{\rm long}$ component and $v_{\rm ph} = v_A$ for the other two components. Although $v_A \gg c_S$ above the solid line in Fig. 3, the scaled amplitudes of the Alfvén mode are still smaller than of the slow acoustic mode at the selected X location.

Figure 3 also shows that the simulation enters into a stationary stage after about 10-15 min. A snapshot of the wave field developed in the stationary stage of the simulations is given in Figure 4. The movie of this simulation is available electronically.

The behaviour of the three wave modes changes across the sunspot radial direction, as expected due to the change of the atmospheric properties. The magnetic field is more inclined at the periphery of the sunspot (much more so than is suggested by the figures, since the vertical scale has been stretched relative to the horizontal scale) and the azimuth varies from $\phi = 0^\circ$ to 180° from the right to the left hand side of the sunspot. The cut-off frequency reaches its maximum of 5.02 mHz at $X = 0$, $Z = 0$ Mm, decreasing steeply above this due to the rise of temperature in the chromosphere (Fig. 2).

This steep temperature increase produces a partial reflection of the slow acoustic mode in the magnetically dominated atmosphere. This reflection is visible as an interference pattern formed above the solid line in the $V_{\rm long}$ projection in the left part of the sunspot (upper panel). This additional reflection also produces stronger slow magnetic modes below the $c_S = v_A$ line in the left part of the sunspot due to the secondary mode transformation from the downgoing waves.

The fast magnetic mode reflection above $c_s = v_A$ is complete in the central part of the sunspot, though the evanescent tail (the exponentially decaying part of the fast wave above the classical reflection point) still does not fully fit in the computational box even here. At the periphery, the height of the simulation domain is insufficient for the fast mode to complete its reflection and it is partly absorbed by the PML boundary condition. This produces artificially large fast mode amplitudes at the periphery of the sunspot.

The Alfvén mode component generated after the transformation is stronger at the horizontal locations where the fast wave is reflected at lower heights ($X = 0$ – 20 Mm). The reason for a this is apparent from Fig. 10b of Cally & Hansen (2011): the fast-to-Alfvén conversion region is distributed throughout the evanescent tail of the fast wave beyond its reflection point. At the frequencies and wavenumbers typical of our simulations here, that amounts to 20 scale heights or more! Since our computational box is truncated only a few scale heights above $z_{\rm ref}$, we can sample only a small part of the conversion process. Where $z_{\rm ref}$ is lower (in the center of Fig. 3c) the Alfvén conversion is of course enhanced relative to where it is higher simply because our box includes more of the conversion region there. Our experiments at 25 mHz, with k_x also increased by a factor of five, confirm this explanation, as for those waves the evanescent tail is much shorter and the conversion region therefore more compact. As expected, the higher frequency simulations yield substantially higher Alfvén fluxes (see Section 6).

4. Energy of three wave modes

We proceed by measuring the energies contained in each of the projected velocity components at the upper part of our simulation domain, above the Alfvén-acoustic equipartition layer $c_S = v_A$. As the properties of the atmosphere change in the horizontal direction across the sunspot, the height of the $c_S = v_A$ layer changes as well (see Fig. 2). To be consistent, we take time averaged energies at heights from 400 km above the $c_S = v_A$ layer up to the upper boundary of our simulation box in the stationary stage of the simulations.

Figure 5 illustrates the energies as a function of inclination and azimuth of the sunspot magnetic field lines at the corresponding horizontal locations. The orientation of the magnetic field is taken at heights where $c_S = v_A$ in each of the simulations at three Y locations. The three strips in each panel of Fig. 5 are for the three simulation runs. The format of the figure allows comparison with the previous studies, Cally & Goossens (2008) Figure 2 and Khomenko & Cally (2011) Figure 4.

This figure demonstrates that the maximum energy of slow acoustic waves is transmitted for inclinations around 30 degrees (left panel). The dependence on the inclination is stronger than the dependence on the azimuth. This result is consistent with previous 2D theoretical models of fast-to-slow mode transformation in the homogeneous inclined magnetic field (Crouch & Cally 2003; Cally 2006; Schunker & Cally 2006). It is also consistent with the 3D analysis by Cally & Goossens (2008). The explanation of this effect is offered by the ray perspective. The fast-mode high-β waves launched from the sub-photospheric layers (with an angle about 90 degrees, i.e. their lower turning point) reach the Alfvén-acoustic equipartition layer with an angle close to $20 - 30$ degrees (Schunker & Cally 2006). Thus, for the moderately inclined magnetic field the attack angle between the wavevector and the magnetic field lines is small and the transformation is efficient. Note also that the frequency of waves is just at the cut-off frequency of the sunspot atmosphere, so due to tunneling effects the slow mode acoustic energy is also present over the wide range of inclinations.

The maximum energy of the Alfvén wave is present at inclinations about 35° and azimuth between 70° and 100° (right panel of Fig. 5). The maximum power increases from the outer to the inner strip indicating a tendency towards larger transmission at larger inclinations. Thus, the behaviour of waves in sunspot models is similar to the one found previously in the models with homogeneous field (Cally & Goossens 2008; Khomenko & Cally 2011; Cally & Hansen 2011). The transmission of Alfvén waves is more efficient for inclined fields, which is important in the sunspot penumbra.

Some transmitted energy is also present in the $E_{\rm trans}$ component (middle panel of Fig. 5) near the sunspot periphery, though we believe this to be an artefact of our computational

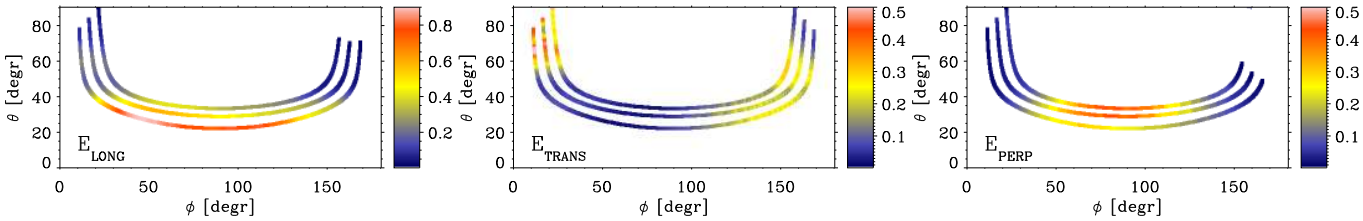

Fig. 5.— Wave energies calculated according to Eq. 10 at the top of the atmosphere (averages at heights from 0.4 Mm above the $c_S = v_A$ layer up to $z = 1.9$ Mm) for the three projected velocity components in turn, selecting respectively acoustic, fast, and Alfvén waves. The units of the color coding are 10^6 erg cm^{-2} s^{-1}. The three strips in each panel are the results of the three simulation runs at $Y = 7.5$ (lower), 11.25 (middle) and 15 Mm (upper) from the sunspot axis.

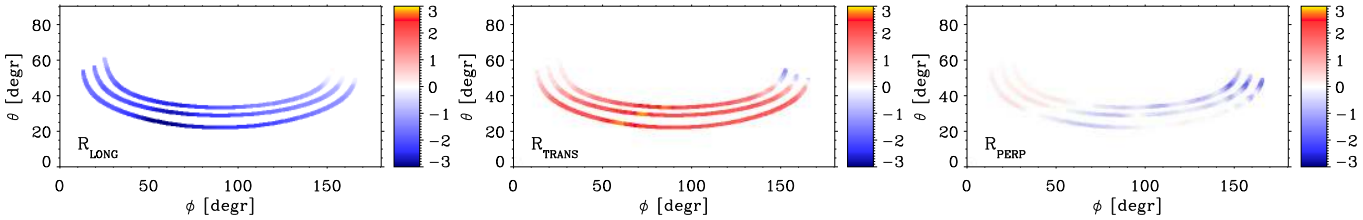

Fig. 6.— Log_{10} of the amplitude ratio $\delta B/\sqrt{\mu_0\rho_0}$ to δV, both projected into the characteristic directions according to Eq. 8. Left panel: slow acoustic mode ($\hat{e}_{\mathrm{long}}$); middle panel: fast magnetic mode ($\hat{e}_{\mathrm{tran}}$); right panel: Alfvén mode ($\hat{e}_{\mathrm{perp}}$). The three strips in each panel are the results of the three simulation runs at $Y = 7.5$ (lower), 11.25 (middle) and 15 Mm (upper) from the sunspot axis.

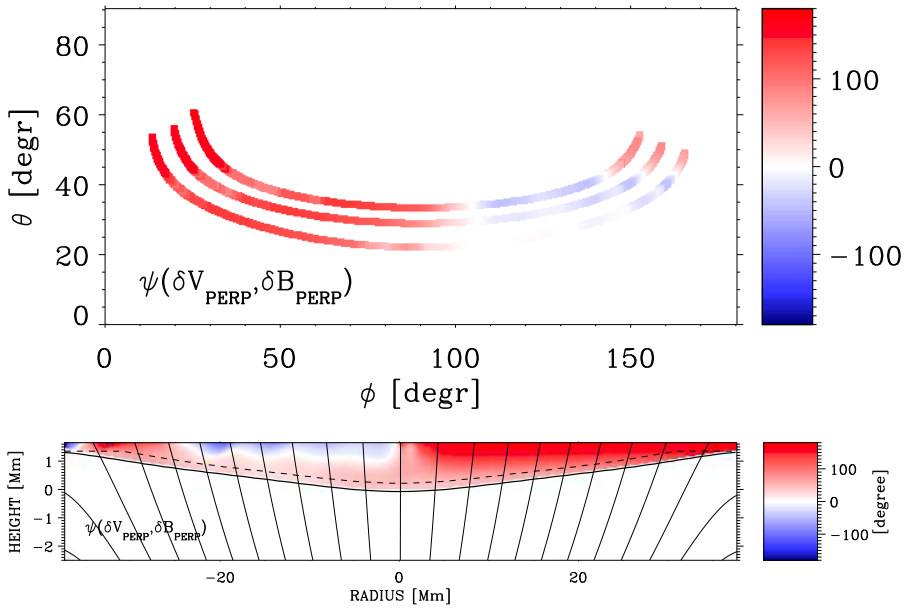

Fig. 7.— Upper panel: phase shift between the variations of $\delta V_{\rm perp}$ and $\delta B_{\rm perp}$ projections. The format is the same as Fig. 6. Lower panel: same quantity, but as a function of height and horizontal distance in the simulation at $Y = 7.5$ Mm from the axis. The phase shift is only shown above the Alfvén-acoustic equipartition layer, where the projections allow the separation between the modes and where the Alfvén mode exists after the transformation.

box not being tall enough to allow complete fast wave reflection there.

5. Alfvén mode polarization relations

To check if projecting the velocities in the directions given by Eq. (8) gives an efficient way to separate the Alfvén mode from the fast and slow magneto-acoustic modes, we make use of the polarization relations for the Alfvén wave. In a classical Alfvén wave variations of the magnetic field and velocity should be related as (see Priest 1984):

$$\delta\vec{V} = \mp\frac{\delta\vec{B}}{\sqrt{\mu_0\rho_0}}\,, \tag{11}$$

where the upper sign is for Alfvén waves propagating parallel to the magnetic field and the lower sign is for those propagating in the opposite direction. The kinetic and magnetic energy for an Alfvén wave should be in equipartition, so the ratio $R = \delta B/\sqrt{\mu_0\rho_0}/\delta V$ should be equal to one.

To confirm the Alfvén nature of the transformed waves, we checked the amplitude and phase relations for all three modes reaching the upper atmosphere. Figure 6 presents calculations of the amplitude ratio R for the three modes. In each of the cases δB and δV pairs are the projections in the corresponding characteristic direction for each mode (Eq. 8). The ratio is taken at the same heights as the energies from Fig. 5 and is averaged in time in the stationary stage of the simulations. The ratio turns out to be different for the three modes. In the case of the slow acoustic mode (left panel), the magnetic field variations associated with the velocity variations are very small (ratio R about 10^{-2}). In contrast, in the case of the fast magnetic mode, magnetic field amplitudes are relatively strong providing the ratio about 10^2 (middle panel). For the Alfvén mode the ratio stays around 10^0 (right panel) meaning that the velocity and magnetic field oscillations are in equipartition as expected for an Alfvén wave.

Figure 7 shows the phase shift between the $\delta B_{\rm perp}$ and $\delta V_{\rm perp}$ corresponding to the Alfvén mode. The situation here is very different from what one might naïvely expect. It is also different to the case of the simple atmosphere and homogeneous magnetic field considered by us previously in Khomenko & Cally (2011). In the right part of the sunspot, for the azimuth between 0° and 90° the Alfvén waves mostly behave as they should. The phase shift is about 180°, meaning an upward wave propagation. Nevertheless, in the left part of the sunspot (ϕ between 90° and 180°) the value of the phase shift indicates a downward propagation. Taking into account that the amplitude ratio (Fig. 6) gives clear evidence for the Alfvénic nature of the waves, we conclude that for ψ between 90° and 180° downward-propagating

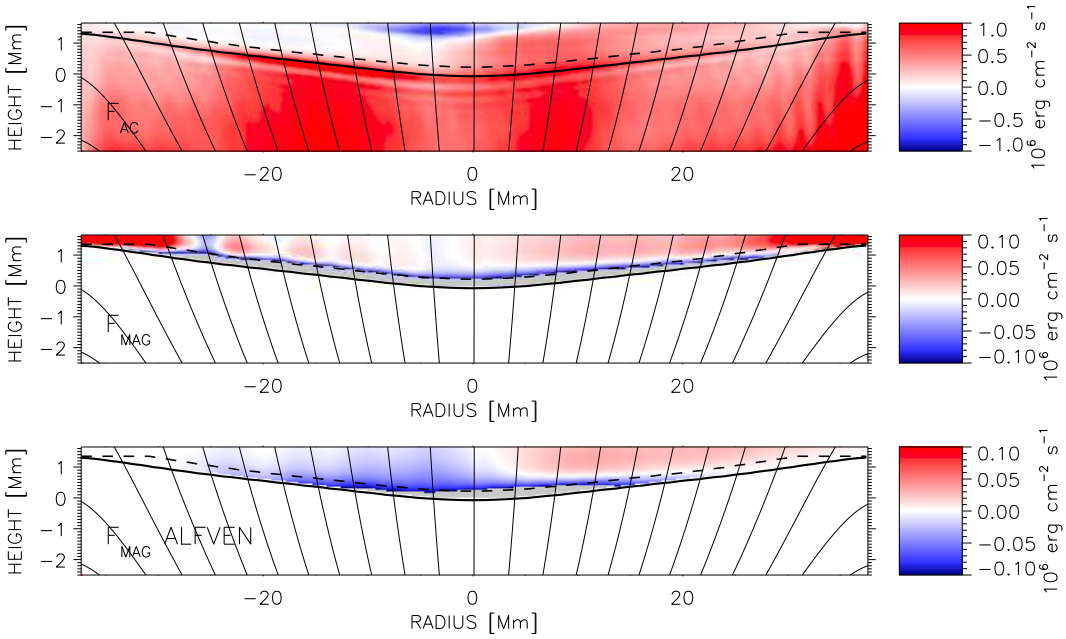

Fig. 8.— Vertical component of the energy fluxes calculated after Eq. 9. Upper panel: acoustic flux; Middle panel: magnetic flux; Bottom panel: magnetic flux, but using $\delta B_{\rm perp}$, $\delta V_{\rm perp}$ in Eq. 9, i.e. magnetic flux due to Alvén waves. In the two bottom panel only values above the Alfvén-acoustic equipartition layer are shown where they are meaningful. Red colors mean upward flux, blue colors mean downward flux.

Alfvén waves are generated by the mode transformation.

This accords perfectly with the uniform field modeling results of Cally & Hansen (2011) (see their Figures 4 and 5) indicating that between 0° and 90° the upward propagating fast waves couple most efficiently to upward Alfvén waves. Since an alignment is needed between the direction of the wave propagation and magnetic field for efficient coupling, where the azimuth is between 90° and 180° the strongest coupling happens between the downward propagating fast waves (after their reflection in the magnetically dominated atmosphere) and the Alfvén waves. In this case downward propagating Alfvén waves are produced. We believe the same happens in the simulations, producing downward propagating Alfvén waves in the left part of the sunspot for ψ above 90°.

All in all these calculations confirm the Alfvén nature of waves selected by the $\hat{e}_{\rm perp}$ projection in our simulations, including returning the predicted result regarding the coupling between refracted fast waves and downward propagating Alfvén waves in regions where the magnetic alignment is favourable.

6. Energy fluxes

We proceed by calculating the acoustic and magnetic fluxes according to Eq. (9). Figure 8 gives the time averages of the vertical magnetic and acoustic fluxes over the upper part of the simulation domain. In the case of the magnetic fluxes we only show them above the Alfvén-acoustic equipartition layer where they are produced and where the separation between the modes according to Eq. (8) is meaningful.

Above the equipartition layer, the upward acoustic flux is mostly present in the right part of the sunspot for intermediate field inclinations (upper panel). This result is in agreement with the energy calculations from Fig. 5 where the maximum of the transmitted acoustic energy is for inclinations about 30°. In the left part of the sunspot the acoustic flux is about zero or slightly negative. A large negative flux is also present at the central part around the axis at the very top of the simulation domain. Thus, slow acoustic waves are reflected in the left part of the sunspot. This appears to be in agreement with the visual impression from Fig. 4 (upper panel) where the interference pattern of the slow acoustic modes is observed to the left of the axis. We believe that this partial reflection is due to steep temperature increase around the axis in the upper chromospheric part of the simulation domain. We have performed additional simulations placing the upper boundary of the domain at lower heights, below the chromospheric temperature increase. In this case we did not observe downgoing slow acoustic waves. This confirms that the reflection is a physical effect and not a numerical

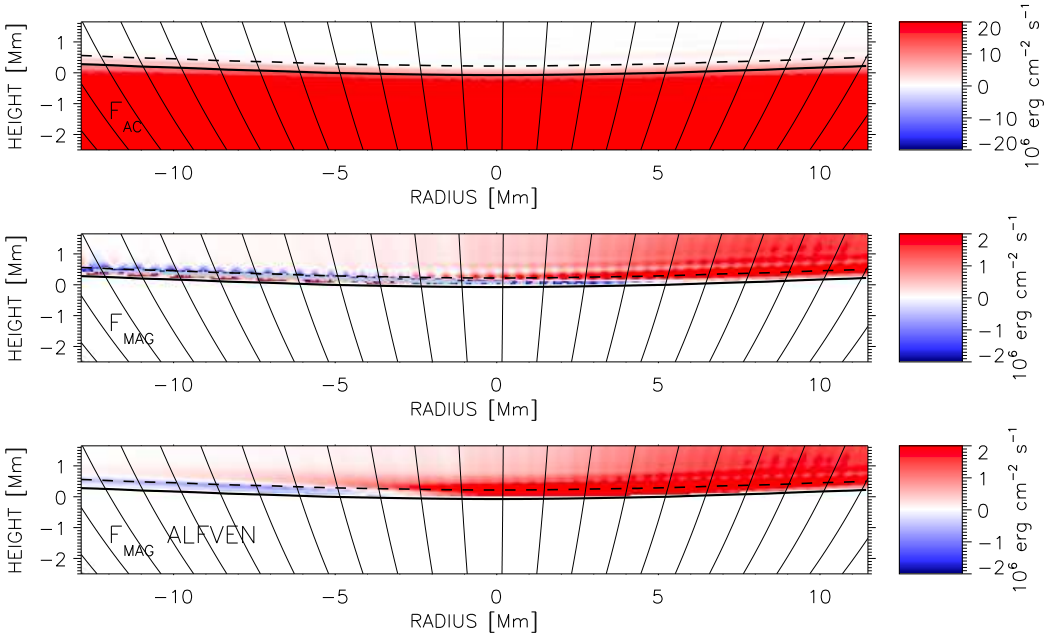

Fig. 9.— Similar to Fig. 8, but for a 25 mHz wave with $k_x = 6.85$ Mm^{-1}. The higher wavenumber shortens the evanescent tail of the fast wave and therefore the Alfvén conversion region is more compact and fits within the computational box. A narrower box and three times finer horizontal resolution has been used here to numerically resolve short-period waves.

artefact from the upper boundary condition of the simulations.

The magnetic flux above the Alfvén-acoustic equipartition layer (middle panel of Fig. 8) is mostly positive. Note that the absolute value of the magnetic flux is at all locations lower than the acoustic flux. The exception is the peripheral regions of the sunspot model where relatively large magnetic flux is obtained. However, this artificially large flux is due to insufficient height of the simulation box above the equipartition layer making it impossible to complete the reflection for the fast magnetic modes.

The magnetic flux in the middle panel of Fig. 8 is due to a mixture of the fast and Alfvén modes. To separate the flux of the Alfvén mode we calculated the magnetic flux from Eq. (9) using the projections $\delta B_{\rm perp}$ and $\delta V_{\rm perp}$. The result is given in the bottom panel of Fig. 8. In agreement with previous considerations we observe that there is no significant flux in the peripheral part of the sunspot, confirming its origin due to incomplete reflection of the fast magnetic mode. As was already clear from the calculation of the phase relations (Fig. 7) the Alfvén flux in the right part of the sunspot (ψ between 0° and 90°) is positive and the flux in the left part of the sunspot (ψ between 90° and 180°) is negative, indicating downward propagating Alfvén waves. These downward propagating waves are generated due to the coupling between the downgoing fast magnetic mode (after its reflection) and the Alfvén mode.

The Alfvén flux only represents a minor fraction of the acoustic flux in Fig. 8. However, as explained at the end of Section 3, we believe this to be an artefact of the truncation of the broad Alfvén conversion region. To overcome this limitation, we performed an experiment with five times larger frequency ($\nu = 25$ mHz) and horizontal wavenumber ($k_x = 6.85$ Mm^{-1}) allowing us to significantly compact the conversion region. This high frequency experiment is illustrated in Fig. 9, where indeed the upward Alfvénic flux in the right half of the region now greatly exceeds the acoustic flux, and there is significant but very compact downward Alfvén flux in the left half. Thus, the conclusion is that Alfvén flux can actually exceed acoustic flux. Besides, Alfvén waves are more able to propagate to great heights than are acoustic or fast waves, which are limited respectively by shock formation and by reflection. This suggests that they do indeed represent a significant product of wave propagation and conversion in sunspots.

7. Conclusions

In this paper we have investigated the efficiency of conversion from fast to Alfvén waves by means of 2.5D numerical simulations in a complex sunspot-like magnetic field configu-

ration. It is important to realize that quantitatively simulating mode transformation numerically is a challenge, as any numerical inaccuracies are amplified in such second-order quantities as wave energy fluxes. The tests presented in this paper prove the robustness of our numerical procedure and offer an effective way to separate the Alfvén from magneto-acoustic modes in numerical simulations.

In general, the conclusions from the previous models in simplified uniform magnetic field configurations (Cally & Goossens 2008; Khomenko & Cally 2011; Cally & Hansen 2011) apply also to our more complex sunspot-like magnetic field configuration, though there are some apparent differences. We note three points in particular.

Firstly, the maximum of the magnetic energy of Alfvén waves transmitted to the upper atmosphere is shifted toward more inclined fields compared to the homogeneous field case.

Secondly, the amount of magnetic energy due to Alfvén waves transmitted to the upper atmosphere is about 10 times lower than for the acoustic waves. This differs from the conclusions reached by Cally & Goossens (2008) who find that at some particular inclinations and azimuth angles the magnetic flux is larger. This discrepancy is entirely to be expected, and is an artefact of the limitations of our present simulations. As seen in Figure 10b of Cally & Hansen (2011), the fast-to-Alfvén conversion region for frequencies comparable to our 5 mHz is spread more or less uniformly over some 20 scale heights from $z_{\rm ref}$ upwards. Clearly, we do not have the luxury of such abundant space in our simulation box, and so only a small fraction of the total potential Alfvén flux is produced. In theory, this could be remedied in any of several ways:

1. The box could be made substantially taller. However, this would involve encompassing yet larger Alfvén speeds, especially if a transition region is included, with unfortunate consequences for our numerical time-step and therefore for the practical feasibility of the calculation.

2. The magnetic field could be increased in magnitude. This is an attractive course of action in any case, as the 900 G at $Z = 0$ adopted here on the axis is very conservative, being a factor of 3 less than might be expected in a mature large sunspot. This would lower both the $c_S = v_A$ equipartition surface and the $\omega = v_A k_x$ fast reflection level opening up more space above for mode conversion. Of course, the maximum Alfvén speed would again increase, with implications for the numerical time step.

3. Higher horizontal wavenumber waves could be modelled, increased by say a factor of 5. As seen in Cally & Hansen (2011), Figure 10b, conversion of waves with $\kappa = k_x H \gtrsim 1$ (where H is the density scale height) occurs in a considerably more compact region

near $z_{\rm ref}$. If frequency is increased by the same factor, then ω/k_x and therefore $z_{\rm ref}$ is unchanged, and the Alfvén conversion region should fit within our computational box. Of course, little power is expected at such high frequencies in the Sun, but nevertheless it is a useful experiment to prove the point. Results of simulations on a similar model but with $k_x = 6.85$ Mm^{-1} and a frequency of 25 mHz are shown in Fig. 9, and are in accord with expectations, yielding far higher Alfvén fluxes.

Finally, where the reflecting fast waves meet similarly inclined magnetic field in the conversion region as they propagate upward, they preferentially transfer their energy to upgoing Alfvén waves. However, if their upward path crosses field lines at large angles there is little transfer. But then this correspondence may be achieved on their way back down, in which case downward propagating Alfvén waves are the beneficiaries of their largess. This more efficient coupling to downward waves happens for azimuth angles above 90°, and was predicted by Cally & Hansen (2011) based on their cold plasma ($\beta = 0$) analysis.

In our future studies we will extend this analysis to fully 3D simulations and include both magnetic field twist and a chromosphere-corona transition region. Of course twist contributes to the field orientation in the conversion regions, and therefore to the strength of mode conversion, both fast-to-slow and fast-to-Alfvén, but we do not anticipate significant novel effects beyond this. On the other hand, a transition region (TR) is expected to be highly reflective to Alfvén waves, and therefore to greatly reduce coronal Alfvén fluxes from chromospheric mode conversion. Results in a zero-β model (Hansen & Cally 2011) confirm this, though they indicate that substantial coronal Alfvén fluxes are still possible if the fast wave reflection point is within a few chromospheric scale heights of the TR, or indeed if the fast wave fails to reflect before it reaches the TR. It will be interesting to test this in realistic sunspot models.

Ultimately, our simulations will inform and be judged against observations of MHD waves in solar magnetic structures. The coronal observations of De Pontieu et al. (2007) and Tomczyk et al. (2007) are useful indicators of power reaching that height, though they are at the limits of our technology and subject to line-of-sight integration ambiguities. Wave observations at photospheric and chromospheric levels may be more reliable and precise. In particular, correlations between velocity and magnetic perturbation phases are crucial in disentangling the various MHD modes in the low atmosphere (Norton et al. 2001; Khomenko et al. 2003; Settele et al. 2002; Fujimura & Tsuneta 2009), though this is a very difficult task even in full 3D simulations.

Significant progress has recently been made in the identification of wave modes observed in sunspots and other solar magnetic features. On the one hand, simultaneous photospheric and chromospheric spectropolarimetric observations (such as those done with the TIP instru-

ment on Tenerife, Canary Islands; Collados et al. 2007) introduce the possibility of "following" wave propagation with height (Centeno et al. 2009; Felipe et al. 2010b) and obtaining phase shifts between oscillations of magnetic field and velocity (Bellot Rubio et al. 2000). On the other hand, bidimensional spectrometers (as e.g. IBIS instrument; Cavallini et al. 2000, or DOT telescope on La Palma, Canary Islands) allow us to obtain high-resolution 2-dimensional velocity fields at different heights. Such simultaneous observations are crucial for our understanding of the physics of wave propagation in active regions. In sunspot umbrae, where the magnetic field is predominantly vertical, slow field-aligned magneto-acoustic waves are firmly detected and even reproduced in simulations including their particular observed wave pattern (Centeno et al. 2006; Felipe et al. 2011). In regions with an inclined magnetic field (sunspot penumbra and network canopies), a mixture of upward and downward propagating waves is often discovered (Braun & Lindsey 2000; Vecchio et al. 2007; Kontogiannis et al. 2010). At photospheric level, these up- and downgoing waves are, possibly, fast magneto-acoustic waves undergoing a reflection process. In fact, from measured phase shifts between velocity and magnetic field oscillations, Khomenko et al. (2003) found that the contribution of slow mode waves is larger in umbral regions and the contribution of fast mode waves becomes progressively more important toward the umbra-penumbra boundary. Alfvén waves are usually detected higher up in the corona (De Pontieu et al. 2007; Tomczyk et al. 2007). The simulations presented here suggest that the complete decoupling between the fast and Alfvén waves happens in the upper chromosphere, or even above. Since the upcoming acoustic waves on the Sun are uncorrelated, their attack angle with respect to the sunspot magnetic field can be arbitrary, so a mixture of up- and downgoing Alfvén waves will be produced, mostly above regions with inclined magnetic field. Time variations of the chromospheric magnetic fields, together with velocity oscillations, are strongly desirable for the firm detection of Alfvén waves. However, measuring magnetic fields in the chromosphere may be challenging (see, e.g., Manso Sainz & Trujillo Bueno 2010) and actual measurements are scarce. As of today, very few measurements exist in active and quiet chromospheric regions (e.g. Socas-Navarro 2005; Trujillo Bueno et al. 2005; Socas-Navarro 2007; Centeno et al. 2010; Štěpán & Trujillo Bueno 2010). But, as far as we are aware, no time variations have been reported. Further instrumental efforts, developments of chromospheric diagnostic techniques, as well as improved modelling, will be needed to constrain the results of the presented study.

Financial support by the Spanish Ministry of Science through projects AYA2010-18029 and AYA2011-24808 is gratefully acknowledged. Work on this project began during a visit by EK to Monash funded by an internal Monash Bridging Grant.

REFERENCES

Avrett, E. H. 1981, in The Physics of Sunspots, ed. L. E. Cram & J. H. Thomas, Vol. 257, Sunspot, NM, Sacramento Peak Observatory, 235–255

Bellot Rubio, L. R., Collados, M., Ruiz Cobo, B., & Rodríguez Hidalgo, I. 2000, ApJ, 534, 989

Berenger, J. P. 1994, J. Comp. Phys., 114, 185

Braun, D. C. & Lindsey, C. 2000, Solar Phys., 192, 307

Cally, P. S. 2001, ApJ, 548, 473

—. 2006, Phil. Trans. R. Soc. A, 364, 333

—. 2007, Astronomische Nachrichten, 328, 286

Cally, P. S. & Bogdan, T. J. 1997, ApJ, 486, L67

Cally, P. S. & Goossens, M. 2008, Solar Phys., 251, 251

Cally, P. S. & Hansen, S. C. 2011, ApJ, 738, 119

Cavallini, F., Berrilli, F., Cantarano, S., & Egidi, A. 2000, in ESA Special Publication, Vol. 463, The Solar Cycle and Terrestrial Climate, Solar and Space weather, ed. A. Wilson, 607–+

Centeno, R., Collados, M., & Trujillo Bueno, J. 2006, ApJ, 640, 1153

—. 2009, ApJ, 692, 1211

Centeno, R., Trujillo Bueno, J., & Asensio Ramos, A. 2010, ApJ, 708, 1579

Christensen-Dalsgaard, J., Dappen, W., Ajukov, S. V., & 30 co-authors. 1996, Science, 272, 1286

Collados, M., Lagg, A., Díaz Garcí A, J. J., Hernández Suárez, E., López López, R., Páez Mañá, E., & Solanki, S. K. 2007, in Astronomical Society of the Pacific Conference Series, Vol. 368, The Physics of Chromospheric Plasmas, ed. P. Heinzel, I. Dorotovič, & R. J. Rutten, 611–+

Cranmer, S. R. & van Ballegooijen, A. A. 2005, ApJS, 156, 265

Crouch, A. D. & Cally, P. S. 2003, Solar Phys., 214, 201

De Pontieu, B., McIntosh, S. W., Carlsson, M., Hansteen, V. H., Tarbell, T. D., Schrijver, C. J., Title, A. M., Shine, R. A., Tsuneta, S., Katsukawa, Y., Ichimoto, K., Suematsu, Y., Shimizu, T., & Nagata, S. 2007, Science, 318, 1574

Felipe, T., Khomenko, E., & Collados, M. 2010, ApJ, 719, 357

—. 2011, ApJ, 735, 65

Felipe, T., Khomenko, E., Collados, M., & Beck, C. 2010b, ApJ, 722, 131

Fujimura, D. & Tsuneta, S. 2009, ApJ, 702, 1443

Hanasoge, S. M., Komatitsch, D., & Gizon, L. 2010, A&A, 522, A87+

Hansen, S. C. & Cally, P. S. 2009, Sol. Phys., 255, 193

—. 2011, ApJ, in preparation

Jefferies, S. M., McIntosh, S. W., Armstrong, J. D., Bogdan, T., Thomas, J., Cacciani, A., & Fleck, B. 2006, ApJ, 648, L151

Khomenko, E. 2009, in ASP Conf. Series, ed. M. Dikpati, T. Arentoft, I. González Hernández, C. Lindsey, & F. Hill, Vol. 416, 31

Khomenko, E. & Cally, P. 2011, in GONG 2010 / SOHO 24, ed. M. Dikpati, T. Arentoft, I. González Hernández, C. Lindsey, & F. Hill, Journal of Physics, 31

Khomenko, E., Centeno, R., Collados, M., & Trujillo Bueno, J. 2008, ApJ, 676, L85

Khomenko, E. & Collados, M. 2006, ApJ, 653, 739

—. 2008, ApJ, 689, 1379

Khomenko, E., Kosovichev, A., Collados, M., Parchevsky, K., & Olshevsky, V. 2009, ApJ, 694, 411

Khomenko, E. V., Collados, M., & Bellot Rubio, L. R. 2003, ApJ, 588, 606

Kontogiannis, I., Tsiropoula, G., & Tziotziou, K. 2010, A&A, 510, A41+

Manso Sainz, R. & Trujillo Bueno, J. 2010, ApJ, 722, 1416

Mihalas, D. & Mihalas, B. W. 1984, Foundations of Radiation Hydrodynamics (Oxford: Oxford University Press)

Newington, M. E. & Cally, P. S. 2010, MNRAS, 402, 386

Norton, A. A., Ulrich, R. K., & Liu, Y. 2001, ApJ, 561, 435

Parchevsky, K. V. & Kosovichev, A. G. 2007, ApJ, 666, L53

Priest, E. R. 1984, Solar magneto-hydrodynamics (Geophysics and Astrophysics Monographs, Dordrecht: Reidel, 1984)

Schunker, H. & Cally, P. S. 2006, MNRAS, 372, 551

Settele, A., Sigwarth, M., & Muglach, K. 2002, A&A, 392, 1095

Socas-Navarro, H. 2005, ApJ, 631, L167

—. 2007, ApJS, 169, 439

Tomczyk, S., McIntosh, S. W., Keil, S. L., Judge, P. G., Schad, T., Seeley, D. H., & Edmondson, J. 2007, Science, 317, 1192

Trujillo Bueno, J., Merenda, L., Centeno, R., Collados, M., & Landi Degl'Innocenti, E. 2005, ApJ, 619, L191

Štěpán, J. & Trujillo Bueno, J. 2010, ApJ, 711, L133

Van Doorsselaere, T., Nakariakov, V. M., & Verwichte, E. 2008, ApJ, 676, L73

Vecchio, A., Cauzzi, G., Reardon, K. P., Janssen, K., & Rimmele, T. 2007, A&A, 461, L1

Vernazza, J. E., Avrett, E. H., & Loeser, R. 1981, ApJ, 45, 635

Zhugzhda, Y. D. & Dzhalilov, N. S. 1982, A&A, 112, 16